IEICE TRANS. COMMUN., VOL.E86–B, NO.5 MAY 2003

PAPER

Advantage of the ESPRIT Method in Polarimetric Interferometry for Forest Analysis

Koichi SATO[†], *Student Member*, **Hiroyoshi YAMADA**[†a)], *and* **Yoshio YAMAGUCHI**[†], *Regular Members*

SUMMARY Polarimetric SAR interferometry has been successful and attractive for forest parameters (tree height and canopy extinction) estimation. In this paper, we propose to use the ESPRIT algorithm to extract the interferometric phase of local scatterers with polarimetric and interferometric SAR data. Two or three local scattering waves can be extracted at each image patch when a fully polarimetric data set (HH, HV, VV) is available. Furthermore, the ESPRIT can estimate two dominant local scattering centers when only a dual polarimetric data set (e.g., VV and VH) is provided. In order to demonstrate effectiveness the proposed technqiue, we examined the relation between local scattering centers extracted by this method and complex coherence of the coherent scattering model for vegetation cover. The results show that the three-wave estimation can be more accurate than the two-wave case. The extracted interferometric phases with full and dual polarization data sets correspond to effective ground and canopy scattering centers. In this investigation, SIR-C/X-SAR data of the Tien Shan flight-pass are used.

key words: *ESPRIT algorithm, SAR interferometry, radar polarimetry, polarimetric interferometry, forest*

1. Introduction

Recently, radar polarimetry and SAR interferometry have been applied to forest parameter estimation in microwave remote sensing [1]–[5]. Conventional SAR interferometry [2] can create accurate terrain topography. The SAR interferometry is sensitive primarily to the vertical structure of vegetated land surface [8]. On the other hand, radar polarimetry is sensitive essentially to the shape, orientation and dielectric constant of vegetation scatterer, Hence, polarimetric interferometry is more sensitive to distribution of the oriented scatterers than either radar polarimetry or interferometry alone.

Papathanassiou and Cloude have utilized these properties to coherent scattering model of structure over forested terrain, and proposed the polarimetric SAR interferometry [7], [9], [10]. The coherence model based on the complex coherence optimization leads to the inversion algorithm for forest parameter estimation such as tree height, underlying topography and average extinction [7], [10]. However we must solve a complex nonlinear parameter optimization problem in this method. Furthermore, fully polarimetric and interferometric data sets are required to solve the problem [10].

On the other hand, Yamada et al. have proposed an alternative technique based on the ESPRIT algorithm [13] which is known as a high-resolution Direction-of-Arrival estimation technique with an antenna array [11]. When we apply the method to polarimetric and interferometric SAR data analysis, we can directly extract forest parameters (phase of effective scattering centers) without solving nonlinear equations [11]. Remaining forest parameters [10] can be easily calculated when we estimate interferometric phase of the ground and canopy, uppermost layer of the forest.

The objective of this paper is to show advantage of the ESPRIT algorithm in polarimetric and interferometric SAR analysis. The method can resolve local scattering centers according to number of the independent polarization channels. This means that we can extract three local scattering centers with a fully polarimetric data set, and two with a restricted dual polarimetric data set. When the forest structure has dominant scattering centers corresponding to the ground and canopy top, the ESPRIT algorithm can extract them correctly. This is the case of the ideal coherence model. In such a case, we can apply the method to restricted dual polarization data sets as well as fully polarimetric ones. This is one of the advantages of the ESPRIT method. When we consider the distribution of leaves and branches in the actual canopy, we may sometimes say that their distribution is not uniform and has additional scattering center(s) in the canopy layer. The ESPRIT algorithm can resolve an additional scattering center in the fully polarimetric analysis. Hence influence of such a nonuniform distribution in the ESPRIT estimation will be decreased with three scattering center analysis.

ALOS/PALSAR, which will be launched in 2004, is equipped with not only the polarimetric mode but also the fine mode (dual polarization mode). The ESPRIT algorithm will be one of the useful analysis tools for the forthcoming data sets.

The paper is organized as follows. In Sect. 2, we summarize the concept of coherence optimization technique and the coherent scattering model in the polarimetric SAR interferometry [6], [10]. Section 3 describes the estimation method based on the ESPRIT

Manuscript received March 27, 2002.
Manuscript revised August 9, 2002.

[†]The authors are with Niigata University, Niigata-shi, 950-2181 Japan.
a) E-mail: yamada@ie.niigata-u.ac.jp

algorithm. Section 4 shows the results obtained by the proposed and the conventional methods, and discuss their relation. Furthermore, the advantage of the ESPRIT method is discussed. Finally, in Sect. 5, we present the conclusions.

2. Coherent Analysis in Polarimetric Interferometry

2.1 Coherence

Fully polarimetric and interferometric system can measure eight scattering signals using two independent linearly polarized antennas at each end of the baseline. Assuming reciprocal scattering, i.e., $E^{(HV)} = E^{(VH)}$, their polarimetric information can be expressed by the following scattering vectors $\boldsymbol{k}_1$ and $\boldsymbol{k}_2$ [6]:

$$\boldsymbol{k}_i = \frac{1}{\sqrt{2}} \begin{bmatrix} E_i^{(HH)} + E_i^{(VV)} \\ E_i^{(HH)} - E_i^{(VV)} \\ 2E_i^{(HV)} \end{bmatrix}, \qquad i = 1 \text{ or } 2. \quad (1)$$

Interferometric coherence between all of these polarimetric combinations can be expressed by using the following coherency matrices,

$$\boldsymbol{T}_{11} = \left\langle \boldsymbol{k}_1 \boldsymbol{k}_1^{*T} \right\rangle, \quad (2)$$

$$\boldsymbol{T}_{22} = \left\langle \boldsymbol{k}_2 \boldsymbol{k}_2^{*T} \right\rangle, \quad (3)$$

$$\boldsymbol{\Omega}_{12} = \left\langle \boldsymbol{k}_1 \boldsymbol{k}_2^{*T} \right\rangle \quad (4)$$

where * and ^{T} indicate complex conjugation and transpose operation, respectively. $\boldsymbol{T}_{11}$ and $\boldsymbol{T}_{22}$ represent polarimetric properties, while $\boldsymbol{\Omega}_{12}$ contains both polarimetric and interferometric information. Then introducing two complex unitary weight vectors $\boldsymbol{w}_1$ and $\boldsymbol{w}_2$, that can be interpreted as the scattering mechanisms, the complex coherence is defined by [6]

$$\tilde{\gamma}(\boldsymbol{w}) = \frac{\left\langle \boldsymbol{w}_1^{*T} \boldsymbol{\Omega}_{12} \boldsymbol{w}_2 \right\rangle}{\sqrt{\left\langle \boldsymbol{w}_1^{*T} \boldsymbol{T}_{11} \boldsymbol{w}_1 \right\rangle \left\langle \boldsymbol{w}_2^{*T} \boldsymbol{T}_{22} \boldsymbol{w}_2 \right\rangle}}. \quad (5)$$

2.2 Coherence Optimization

The optimized coherence is obtained by finding scattering mechanisms, $\boldsymbol{w}_1$ and $\boldsymbol{w}_2$, that maximize the interferometric coherence defined in Eq. (5). This is equivalent to solve complex eigenvalue problems with common eigenvalues ν_i, [6]

$$\boldsymbol{T}_{11}^{-1} \boldsymbol{\Omega}_{12} \boldsymbol{T}_{22}^{-1} \boldsymbol{\Omega}_{12}^{*T} \boldsymbol{w}_{1i} = \nu_i \boldsymbol{w}_{1i}, \quad (6)$$

$$\boldsymbol{T}_{22}^{-1} \boldsymbol{\Omega}_{12}^{*T} \boldsymbol{T}_{11}^{-1} \boldsymbol{\Omega}_{12} \boldsymbol{w}_{2i} = \nu_i \boldsymbol{w}_{2i}. \quad (7)$$

The eigenvalues are real. The optimized coherence is given by the maximum eigenvalue $\tilde{\gamma}_{max} = \sqrt{\nu_{max}}$. Using the eigenvalues, Eqs. (6) and (7) can also be rewritten as follows:

$$\begin{aligned} &\boldsymbol{T}_{11}^{-1} \boldsymbol{\Omega}_{12} \boldsymbol{T}_{22}^{-1} \boldsymbol{\Omega}_{12}^{*T} \\ &\quad = \nu_1 (\boldsymbol{w}_{11} \boldsymbol{w}_{11}^{*T}) + \nu_2 (\boldsymbol{w}_{12} \boldsymbol{w}_{12}^{*T}) \\ &\qquad + \nu_3 (\boldsymbol{w}_{13} \boldsymbol{w}_{13}^{*T}), \end{aligned} \quad (8)$$

$$\begin{aligned} &\boldsymbol{T}_{22}^{-1} \boldsymbol{\Omega}_{12}^{*T} \boldsymbol{T}_{11}^{-1} \boldsymbol{\Omega}_{12} \\ &\quad = \nu_1 (\boldsymbol{w}_{21} \boldsymbol{w}_{21}^{*T}) + \nu_2 (\boldsymbol{w}_{22} \boldsymbol{w}_{22}^{*T}) \\ &\qquad + \nu_3 (\boldsymbol{w}_{23} \boldsymbol{w}_{23}^{*T}). \end{aligned} \quad (9)$$

Equations (8) and (9) show that the coherence optimization algorithm decompose three independent scattering mechanisms and phase centers which is given by the three pairs of the eigenvectors $(\boldsymbol{w}_{1i}, \boldsymbol{w}_{2i})$. It is often called coherent scattering decomposition [6]. In forest observations, if the characteristic polarization state of the volume scattering in the canopy layer is orthogonal to that of the ground scattering, the algorithm leads to the effective forest height.

2.3 Coherence Model in Forest

For forest observation at L- and P-Band radars, the received signals contain both the ground and canopy scattering components. Then, when simple random volume scatterings are assumed due to spatially distributed particles such as leaves and branches in canopy over ground, the complex coherence can be written by [7], [10]

$$\tilde{\gamma}(\boldsymbol{w}) = e^{j\phi_0} \frac{\tilde{\gamma}_V + m(\boldsymbol{w})}{1 + m(\boldsymbol{w})}, \quad (10)$$

where ϕ_0 is an underlying topographic phase, $\tilde{\gamma}_V$ is the complex coherence due to volume scattering, and $m(\boldsymbol{w})$ is ratio of the ground to the volume scattering amplitudes. Temporal decorrelation is assumed to be negligibly small. The coherence model is a function of the ground-to-volume scattering ratio $m(\boldsymbol{w})$ where $\boldsymbol{w}$ denotes the unitary scattering mechanism vector [7]. Equation (10) can be also rewritten as

$$\tilde{\gamma}(\boldsymbol{w}) = e^{j\phi_0} \left[\tilde{\gamma}_V + \frac{m(\boldsymbol{w})}{1 + m(\boldsymbol{w})} (1 - \tilde{\gamma}_V) \right]. \quad (11)$$

This equation shows that any $\tilde{\gamma}(\boldsymbol{w})$ appear on a straight line passing through the point $\tilde{\gamma}_V$ with direction $(1 - \tilde{\gamma}_V)$ in the complex plane. This geometrical representation is shown in Fig. 1. Therefore, the observable coherences, denoted by $\tilde{\gamma}(\boldsymbol{w}_1)$, $\tilde{\gamma}(\boldsymbol{w}_2)$, and $\tilde{\gamma}(\boldsymbol{w}_3)$ as examples, lie on the this line.

In the extreme case $m = \infty$ or $m = 0$, we can obtain the coherence of the ground or the canopy scattering only. The typical ground reflection components are single bounce reflections by the ground and two double bounce reflections (the ground-trunk reflection and the ground-canopy reflection). The ideal canopy modeled as random dipole clouds has completely depolarized component only. As the results, polarization state of the volume scattering is orthogonal to that of the ground scattering in this ideal model [7].

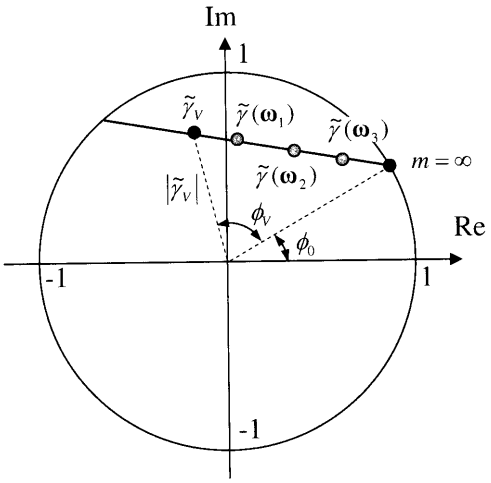

Fig. 1 Geometrical representation of the coherence model.

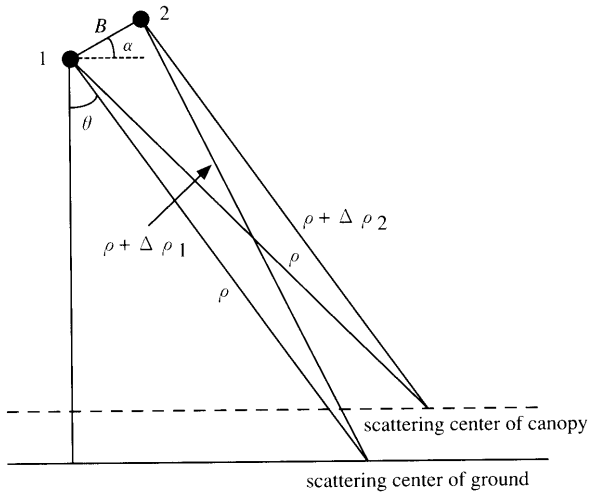

Fig. 2 Interferometric geometry of two scattering centers model.

2.4 Parameter Inversion

Inversion problem of forest parameters based on Eq. (10) has six unknowns $(\phi_0, \phi_V, |\tilde{\gamma}_V|, m_1, m_2, m_3)$. In this problem, ϕ_V is the key parameter which determines the effective forest height. However the independent observables with fully polarimetric interferometric system are three complex coherences (e.g., HH, HV(=HV), VV or three the optimized coherences). Therefore, we have to solve the six-dimensional nonlinear optimization problem defined by [7], [10]

$$\min\left(\left\|\begin{bmatrix}\tilde{\gamma}_1\\ \tilde{\gamma}_2\\ \tilde{\gamma}_3\end{bmatrix} - [M]\begin{bmatrix}e^{j\phi_0}\\ e^{j\phi_V}\\ |\gamma_V|\\ m_1\\ m_2\\ m_3\end{bmatrix}\right\|\right), \tag{12}$$

where the operator $[M]$ indicates the physical scattering model. The inversion algorithm often employs three optimized coherences provided by the coherence optimization in order to improve the solving condition [10].

3. ESPRIT Method

In this section, we assume repeat-pass observation of forest region. Figure 2 shows the interferometric geometry in this case. The observed backscattered data can be modeled by the sum of dominant scattering centers located on the ground and in the canopy. Thus the received signals using kl polarization (e.g., HH, HV and VV) in orbit-1 and orbit-2 may be written by [11]

$$E_1^{(kl)} = \sum_{i=1}^{d} \sigma_i s_i^{(kl)} e^{j\frac{4\pi}{\lambda}\rho} + n_1^{(kl)} \tag{13}$$

$$E_2^{(kl)} = \sum_{i=1}^{d} \sigma_i s_i^{(kl)} e^{j\frac{4\pi}{\lambda}(\rho+\Delta\rho_i)} + n_2^{(kl)} \tag{14}$$

where d denotes the number of extracting dominant component in the local patch, σ_i is the complex amplitude of the i-th scattering wave, and $s_i^{(kl)}$ is the polarization state of i-th local scatter in kl polarization. Each polarization state is assumed to be normalized with respect to σ_i. ρ and $\Delta\rho_i$ are the slant-range distance from the orbit-1 to the range bin, and the slant-range difference of the scatter, respectively. $n_1^{(kl)}$ and $n_2^{(kl)}$ are the additive noise of kl channel at orbit-1 and orbit-2, respectively.

Rewriting Eq. (13) and (14) in vector notation, we obtain

$$\boldsymbol{E}_1 = \left[E_1^{(HH)}, E_1^{(HV)}, E_1^{(VV)}\right]^T = \boldsymbol{S}\boldsymbol{\sigma} + \boldsymbol{n}_1 \tag{15}$$

$$\boldsymbol{E}_2 = \left[E_2^{(HH)}, E_2^{(HV)}, E_2^{(VV)}\right]^T = \boldsymbol{S}\boldsymbol{D}\boldsymbol{\sigma} + \boldsymbol{n}_2 \tag{16}$$

the $M \times d$ matrix $\boldsymbol{S}$ contains the polarization state of each local scatter. $\boldsymbol{\sigma}$ is a $d \times 1$ vector of the complex amplitudes $\sigma_i e^{j4\pi\rho/\lambda}$, and $\boldsymbol{D}$ is a $d \times d$ diagonal matrix whose element contains phase differences between orbit-1 and orbit-2, i.e., interferometric phase. $\boldsymbol{n}_1$ and $\boldsymbol{n}_2$ are the noise vectors. In the followings, we explain an outline of the TLS (Total Least Square) ESPRIT briefly.

In the TLS-ESPRIT algorithm [13], the total overall vector $\boldsymbol{x}$ and its correlation matrix $\boldsymbol{R}_{xx}$ are defined as

$$\boldsymbol{x} = \begin{bmatrix}\boldsymbol{E}_1\\ \boldsymbol{E}_2\end{bmatrix} = \begin{bmatrix}\boldsymbol{S}\\ \boldsymbol{S}\boldsymbol{D}\end{bmatrix}\boldsymbol{\sigma} + \begin{bmatrix}\boldsymbol{n}_1\\ \boldsymbol{n}_2\end{bmatrix} \tag{17}$$

$$\boldsymbol{R}_{xx} = \left\langle \boldsymbol{x}\boldsymbol{x}^{*T} \right\rangle. \tag{18}$$

The eigenvalues of $\boldsymbol{R}_{xx}$ have following property

$$\lambda_1 \geq \lambda_2 \geq \cdots \lambda_d > \lambda_{d+1} = \cdots = \lambda_{2M} (= \sigma_N^2). \tag{19}$$

where σ_N^2 is the noise power, and M indicates the number of paired ($M = 4$ in Eqs. (13) and (14)). The

number of dominant scatterer can be estimated by this property. In forest regions, there are more than two dominant eigenvalues. Therefore it is possible to extract two or three scattering waves using fully-polarimetric data sets.

The matrix $\boldsymbol{D}$ can be estimated using the eigenvectors, $\boldsymbol{e}_1, \cdots, \boldsymbol{e}_d$, that correspond to dominant eigenvalues. The eigenvectors relate to the matrices $\boldsymbol{D}$ and $\boldsymbol{S}$ such that

$$[\boldsymbol{e}_1, \boldsymbol{e}_2, \cdots, \boldsymbol{e}_d] \triangleq \begin{bmatrix} \boldsymbol{F}_1 \\ \boldsymbol{F}_2 \end{bmatrix} = \begin{bmatrix} \boldsymbol{SC} \\ \boldsymbol{SDC} \end{bmatrix} \tag{20}$$

where $\boldsymbol{C}$ is a $d \times d$ non-singular matrix. Here, we define a matrix $\boldsymbol{F}_{12}$ as

$$\boldsymbol{F}_{12} = [\boldsymbol{F}_1, \boldsymbol{F}_2]. \tag{21}$$

There exists a unique $2d \times d$ matrix $\boldsymbol{G}$ which satisfies the following equation

$$\begin{aligned} \boldsymbol{0} &= \boldsymbol{F}_{12}\boldsymbol{G} = \boldsymbol{F}_1\boldsymbol{G}_1 + \boldsymbol{F}_2\boldsymbol{G}_2 \\ &= \boldsymbol{STG}_1 + \boldsymbol{SDTG}_2, \end{aligned} \tag{22}$$

$$\boldsymbol{G} = \begin{bmatrix} \boldsymbol{G}_1 \\ \boldsymbol{G}_2 \end{bmatrix}. \tag{23}$$

The matrix $\boldsymbol{G}$ spans the null-space of $\boldsymbol{F}_{12}$. Defining a matrix $\boldsymbol{\Psi}$:

$$\boldsymbol{\Psi} = -\boldsymbol{G}_1\boldsymbol{G}_2^{-1} \tag{24}$$

and substitutes it into Eq. (22), we obtain

$$\boldsymbol{SC\Psi} = \boldsymbol{SDC}. \tag{25}$$

From these results, $\boldsymbol{D}$ can be easily given by

$$\boldsymbol{D} = \boldsymbol{C\Psi C^{-1}}. \tag{26}$$

Therefore, the eigenvalues $\lambda'_1, \cdots, \lambda'_d$ of $\boldsymbol{\Psi}$ equal to each of interferometric phase ϕ_i

$$\phi_i = \arg(\lambda'_i). \tag{27}$$

Note that the algorithm is applicable to restricted dual-polarization data sets [12]. In this case, the observed data vectors in Eqs. (15) and (16) may be redefine as

$$\boldsymbol{E}_1 = \left[E_1^{(pol1)}, E_1^{(pol2)}\right]^T \tag{28}$$

$$\boldsymbol{E}_2 = \left[E_2^{(pol1)}, E_2^{(pol2)}\right]^T \tag{29}$$

where pol_1 and pol_2 indicate usable polarization channels (e.g., HH, HV).

4. Experimental Results

In this section, we show availability of the ESPRIT algorithm for extracting the interferometric phase of local scatterers in forest with full or restricted dual polarization data sets. In order to show the estimation accuracy, we show the relation between local scattering centers estimated by the ESPRIT method and the complex coherences [10] by the conventional technique. The data are the repeat-pass fully polarimetric and interferometric data pairs at L-Band in the Tien-Shan flight-path acquired by the SIR-C/X-SAR system on October 8 and 9, 1994. The evaluated area is shown in Fig. 3. The forest area is located at lower left of the image, and the farmland area is extended from the center to upper region. Also, are shrub-land areas in the upper part around the Selenga River.

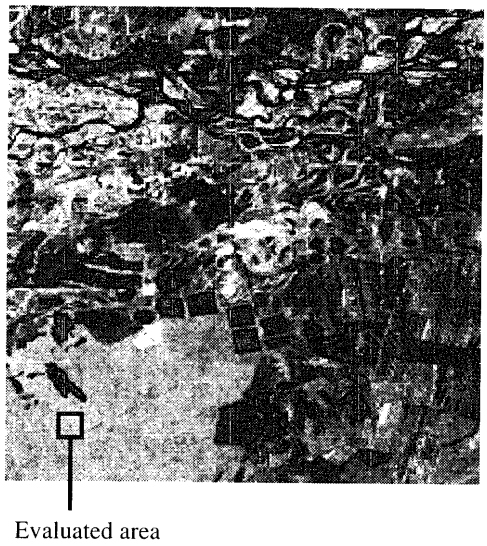

Fig. 3 L-Band total power image of the Tien-Shan flight-path. The rectangular region shows the extracted area for the evaluation in the forest.

To examine the coherence scattering model, we plot the HH-HH, HV-HV and VV-VV coherences and the three optimum coherence values [6] in the complex plane. In the following graphs, we plot three optimized coherences introduced by Ref. [6] as "opt.1," "opt.2," and "opt.3." These coherences can be obtained by maximizing coherences in changing the polarization state of observations. The optimized coherences have the relation:$|\tilde{\gamma}_{opt.1}| \geq |\tilde{\gamma}_{opt.2}| \geq |\tilde{\gamma}_{opt.3}|$. (Please see [6] for the details.) Furthermore, the interferometric phases estimated by the ESPRIT method are marked by partially painted circle markers in Fig. 4(a) and triangular markers in Fig. 4(b) at the related phase location on the unit circle in the complex plane. These phases directly correspond to ϕ_i in (27). Note that the ESPRIT can estimate only interferometric phase of the local scatterers. To estimate effective tree height, the phase information (ϕ_0, ϕ_V) shown in Fig. 1 is required only [10]. The patches 1 and 2 were selected in the "Evaluated area" in Fig. 3. Here, we first apply 4 (1 range and 4 azimuth) multi-look processing to decrease speckle and phase noise effect. Additional 16 multi-look processing (ensemble average) is also applied to evaluate $\boldsymbol{R}_{xx}$ in (18) for the ESPRIT analysis.

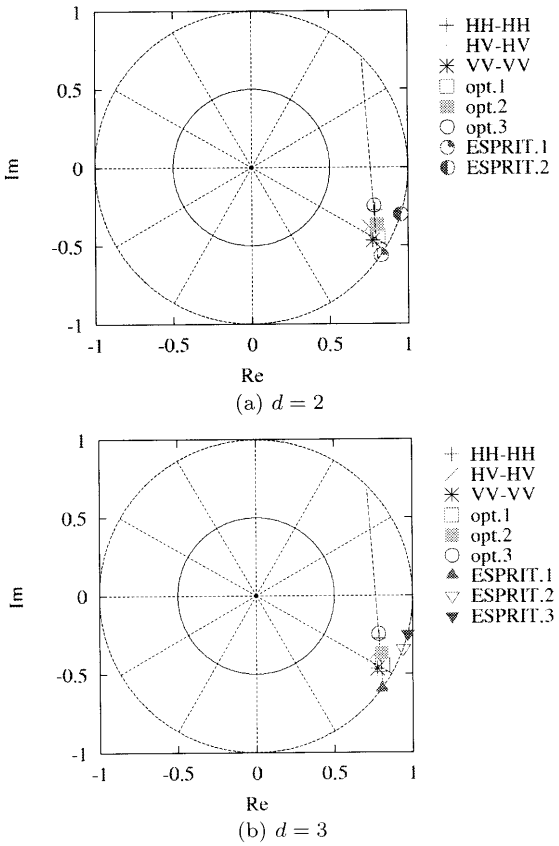

Fig. 4 Distribution of the interferometric phases estimated by the ESPRIT method and the complex coherence values at patch 1.

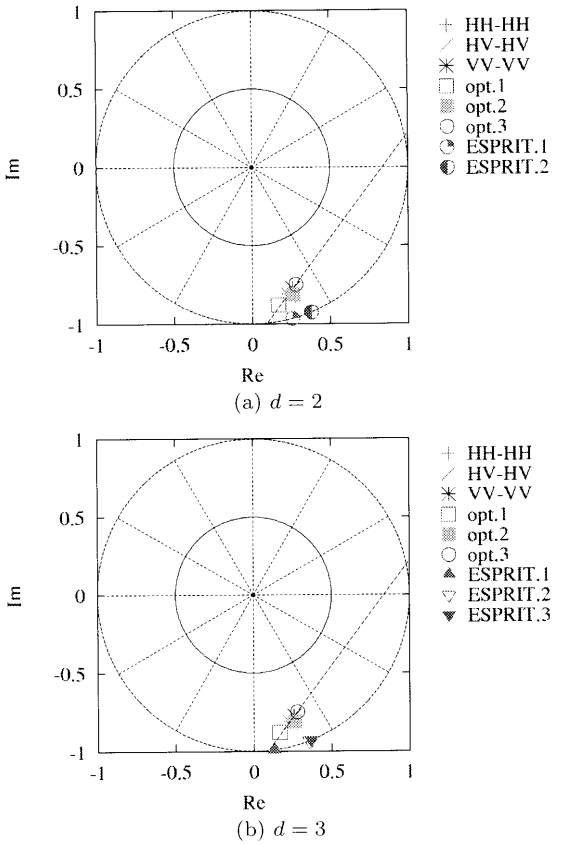

Fig. 5 Distribution of the interferometric phases estimated by the ESPRIT method and the complex coherence values at patch 2.

Since each of the coherences locates on a straight line in Figs. 4 and 5, it can be said that the coherence model holds at each patch. The local interferometric phases extracted by the ESPRIT method with $d = 2$ correspond to the effective ground and canopy scattering centers based on the coherence model, respectively (Fig. 4(a)). Almost the same results can be obtained with $d = 3$ as shown in Fig. 4(b).

On the other hand, the first component by the ESPRIT method with $d = 2$ is different from the ground scattering center with the coherence model at the patch 2 as shown in Fig. 5, and the phase difference between the 1st and the 2nd components is small clearly, the ESPRIT algorithm contain bias in this case. This is because when there exist more than two scattering centers or the widely distributed canopy scattering centers, the two scattering center model is not adequate for the ESPRIT estimation. However, it can be improved using three scattering waves extraction ($d = 3$). It is useful when the power of canopy or ground scattering center has lower than the trunk. Therefore, the accuracy of three-wave estimation is higher than two-wave estimation. Note that the 3rd component is the noise when there are only two dominant scatterer at the patch. Hence, selection of suitable number of scattering centers is important.

Next, the two-wave extractions with restricted dual polarization data sets are carried out at the patch 1, according to Eqs. (28) and (29). Figures 6(a), (b) and (c) show the estimated scattering centers. The ESPRIT.1 and the ESPRIT.2 shown in these figures correspond to the estimated effective scattering centers on the ground and in the canopy, respectively. The "ESPRIT.2" in Fig. 6(b) has almost the same phase as "ESPRIT.2" in Figs. 6(a) and (c). They correspond to phase of canopy scattering center. However, "ESPRIT.1" corresponding to phase of the ground scattering center in Fig. 6(b) was slightly biased in comparison with those in Figs. 6(a) and (c). This may be caused by the low Signal to Noise Ratio (SNR) or the difference of dominant scattering centers at each of the polarizations. Comparing the dual polarization results in Figs. 6 with the fully polarimetric result in Fig. 4, it can be said that the combination of HH and VV data sets (Fig. 6(a)) provides almost the same results as those in Fig. 4. According to Figs. 6, the estimated phases of the ground by the ESPRIT ("ESPRIT.1"s) did not agree well. This can be considered that polarization state of each local scatterer is quite different, hence the selection of combination largely affect the estimation accuracy.

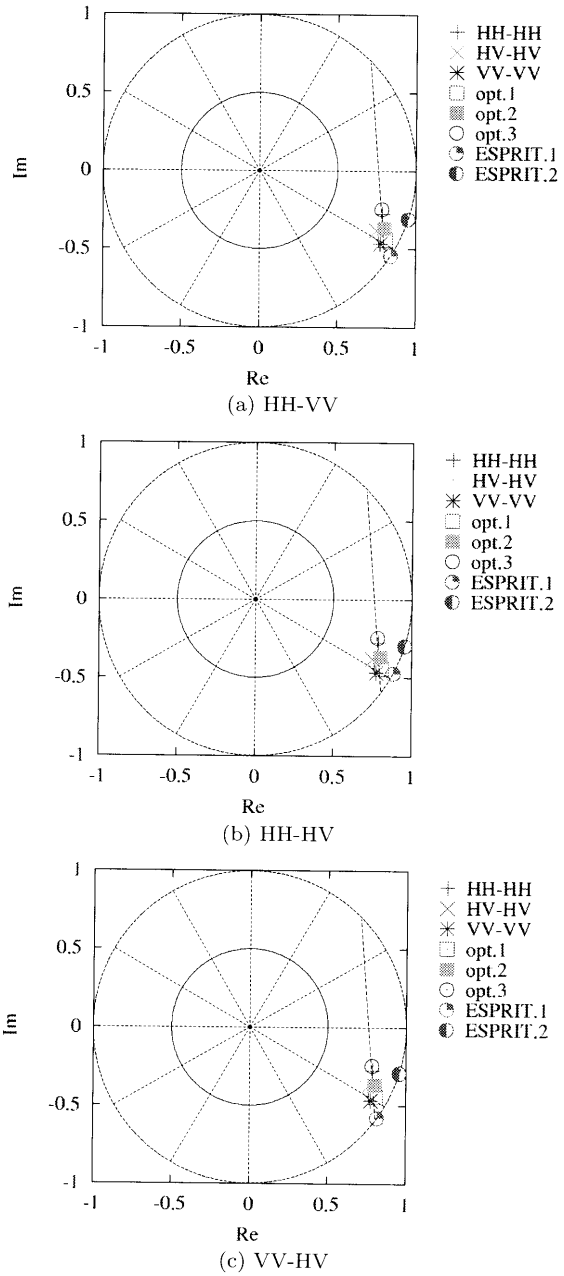

Fig. 6 Distribution of the interferometric phases estimated by the ESPRIT method with dual-polarization data sets and the complex coherence values at patch 1.

The results in this patch show that the ground contribution is weak in HH and HV data, and strong in VV data. Figure 7 shows histograms of differential phase between the ground and canopy of overall forest area in Fig. 3. The forest area can be discriminated by the eigenvalue distribution in (19) [11]. As shown in this figure, results of the dual polarimetric analysis with HH and VV data set and th fully polarimetric analysis agree well. Due to low SNR of the HV data set, the available patches for the ESPRIT analysis decrease, however, peaks of the curves still coincide with the others. These results

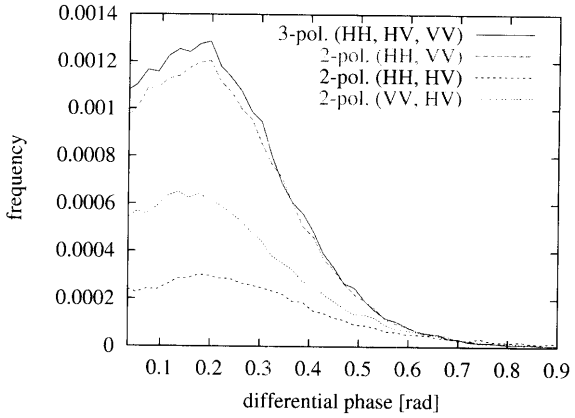

Fig. 7 Histogram of the estimated phase difference between the ground and canopy by the ESPRIT algorithm.

show the possibility of estimation in restricted dual polarization data sets. The detection performance of the dual polarization analysis depends on the combination of polarization, however, the ESPRIT method can detect correct scattering centers using suitable polarization data sets. Selection of optimal polarization combination would be important problem for obtaining good estimation. This will depends on spatial distribution of canopy scattering centers, or state of forest (e.g., dense or sparse). Quantitative evaluation of estimation accuracy in dual polarization data sets will be done in near future.

5. Conclusions

In this paper, we showed the performance of the ESPRIT algorithm for interferometric phase extraction of local scattering waves. The relation between local scattering centers directly estimated by the ESPRIT method and coherent scattering model is investigate to show the validity of the method. As a result, the three-wave estimation by the ESPRIT method can be more accurate than two-wave and their extracted interferometric phases correspond to effective ground and canopy scattering centers, which lies on a straight line of the coherence model in the complex plane, respectively. Furthermore, the estimation with the dual polarization analysis works properly as well as the two-wave extraction with full polarization data sets. These results are also verified using the data sets acquired by DLR's E-SAR system at L-Band. Hence, the ESPRIT method are widely available to various data sets such as acquired by the ALOS/PALSAR mission which will be launched in 2004.

Acknowledgment

This work in part was supported by Grant-in-Aid for Development Scientific Research from Japan Society for Promotion of Science and Grant for Promotion of Nii-

gata University Research Projects.

References

[1] J. Askne, P.B. Dammert, L.M. Ulander, and G. Smith, "C-band repeat-pass interferometric SAR observations of the forest," IEEE Trans. Geosi. Remote Sens., vol.35, no.1, pp.25–35, Jan. 1997.
[2] R.N. Treuhaft, S.N. Madsen, M. Moghaddam, and J.J. van Zyl, "Vegetation characteristics and surface topography from interferometric radar," Radio Sci., vol.31, pp.1449–1485, Nov./Dec. 1996.
[3] J.O. Hagberg, L.M. Ulander, and J. Askne, "Repeat-pass interferometry over forested terrain," IEEE Trans. Geosci. Remote Sens., vol.33, no.2, pp.331–340, 1995.
[4] S.S. Saatchi and M. Moghaddam, "Estimation of crown and stem water content and biomass of boreal forest using polarimetric SAR imagery," IEEE Trans. Geosi. Remote Sens., vol.38, no.2, pp.697–709, March 2000.
[5] K.J. Ranson and G. Sun, "Effects of environmental conditions on boreal forest classification and biomass estimates with SAR," IEEE Trans. Geosi. Remote Sens., vol.38, no.3, pp.1242–1252, May 2000.
[6] S.R. Cloude and K.P. Papathanassiou, "Polarimetric SAR interferometry," IEEE Trans. Geosi. Remote Sens., vol.36, no.5, pp.1551–1565, Sept. 1998.
[7] K.P. Papathanassiou and S.R. Cloude, "Vegetation and ground parameter estimation using polarimetric interferometry part 1/2," Proc. ESA CEOS SAR Workshop, Toulouse, France, Oct. 1999.
[8] R.N. Treuhaft and P.R. Siqueira, "Vertical structure of vegetated land surfaces from interferometric and polarimetric radar," Radio Sci., vol.35, pp.141–177, Jan./Feb. 1998.
[9] K.P. Papathanassiou, S.R. Cloude, A. Reigber, and W.M. Boerner, "Multi-baseline polarimetric SAR interferometry for vegetation parameter estimation," Proc. IGRASS 2000, pp.24–28, July 2000.
[10] K.P. Papathanassiou and S.R. Cloude, "Single-baseline polarimetric SAR interferometry," IEEE Trans. Geosi. Remote Sens., vol.39, no.11, pp.2352–2363, Nov. 2001.
[11] H. Yamada, Y. Yamaguchi, Y. Kim, E. Rodriguez, and W.M. Boerner, "Polarimetric SAR interferometry for forest analysis based on the ESPRIT algorithm," IEICE Trans. Electron., vol.E84-C, no.12, pp.1917–1924, Dec. 2001.
[12] H. Yamada, Y. Yamaguchi, E. Rodriguez, Y. Kim, and W.M. Boerner, "Polarimetric SAR interferometry for forest canopy analysis by using the super-resolution method," Proc. IGRASS 2001, on CD-ROM, July 2001.
[13] R. Roy and T. Kailath, "ESPRIT—Estimation of signal parameters via rotational invariance techniques," IEEE Trans. Acoust., Speech Signal Process., vol.37, no.7, pp.984–995, July 1989.

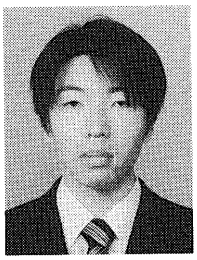

Koichi Sato was born in Niigata Prefecture, Japan, on February 13, 1978. He received the B.E. degree in information engineering from Niigata University, Niigata, Japan, in 2000. He is now a graduate student pursuing the M.E. degree at Niigata University, where he is engaged in SAR interferometry and radar polarimetry.

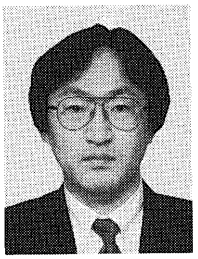

Hiroyoshi Yamada received the B.E, M.E. and Dr.Eng. degrees from Hokkaido University, Sapporo, Japan, in 1988, 1990 and 1993, respectively, all in electronic engineering. In 1993, he joined the Faculty of Engineering, Niigata University, where he is an associate professor. From 2000 to 2001, he was a Visiting Scientist at Jet Propulsion Laboratory, California Institute of Technology, Pasadena. His current interests involve in the field of array signal processing, radar polarimetry and interferometry, microwave remote sensing and imaging. Dr. Yamada is a member of IEEE.

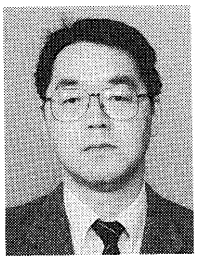

Yoshio Yamaguchi received the B.E. degree in electronics engineering from Niigata University in 1976, and the M.E. and Dr.Eng. degrees from Tokyo Institute Technology in 1978 and 1983, respectively. In 1978, he joined the Faculty of Engineering, Niigata University, where he is a professor. From 1988 to 1989, he was a Research Associate at the University of Illinois, Chicago. His interests are in the field of propagation characteristics of electromagnetic waves in lossy medium, radar polarimetry, microwave remote sensing and imaging. Dr. Yamaguchi is a fellow of IEEE, and a member of the Japan Society for Snow Engineering.